Journal of Building Engineering 103 (2025) 112072

Contents lists available at ScienceDirect

Journal of Building Engineering

journal homepage: www.elsevier.com/locate/jobe

Glass fibre-based FRCM systems under mild temperature exposures

Matteo Canestri *, Francesca Ferretti, Claudio Mazzotti

Department of Civil, Chemical, Environmental and Materials Engineering, University of Bologna, Viale Risorgimento 2, 40136, Bologna, Italy

ARTICLE INFO

Keywords:
FRCM systems
Tensile behaviour
Temperature
Single-lap direct shear
Glass fibres
Aramid fibres

ABSTRACT

Fibre Reinforced Cementitious Matrix (FRCM) systems have been widely used as an effective method for retrofitting existing structures. However, their durability against environmental actions remains partially unsolved. A comprehensive experimental study was carried out to investigate the influence of different temperature levels on the mechanical properties of two FRCM systems. The first system was composed of a combination of aramid and glass fibres as reinforcing textile, while the second system was strengthened with glass fibres only. Tests were carried out on dry bundles and textiles, mortar prisms, FRCM coupons and single-lap direct shear specimens. A specific thermal procedure was developed and employed to control the conditioning and testing phases. To investigate the impact of temperature exposure on the tensile and bond behaviour of the FRCM systems, capacity retention rates were evaluated and, in general, a decreasing trend was registered in terms of peak axial stress *vs* temperature. In terms of tensile properties, a similar negative impact of temperature was registered for both systems, with capacity retention rates ranging between 60 % and 70 % at the highest temperature levels tested. In terms of bond behaviour, temperature variations can potentially trigger a change in the failure mode, which was more pronounced for the system containing only glass fibres, for which lower retention rates were recorded, with a maximum reduction to 50 % at the highest temperature. The obtained outcomes demonstrated how even mild temperatures can potentially affect the tensile strength of these systems as well as their bond capacity when applied on masonry substrates.

1. Introduction

In recent years, the destruction caused by major earthquakes has brought attention to the seismic vulnerability of built heritage. The topic is especially significant in countries with a cultural heritage largely composed of degraded masonry structures [1–7]. This immense legacy must be properly preserved and maintained by applying appropriate strengthening techniques and systems. Firstly, Fiber Reinforced Polymer (FRP) composite system emerged as a valid solution to enhance the load bearing capacity of existing structures, with a large number of studies that concentrated on analysing the debonding mechanism of the interface between the reinforcement and the substrate [8–12]. However, these retrofitting solutions were characterised by a low vapour compatibility and irreversibility of application. For this reason, FRCM systems recently emerged as a valid alternative, characterised by a high strength-to-weight ratio and optimal compatibility with masonry substrates. They are typically applied in thin layers (ranging from 5 to 25 mm, depending on the number of adopted layers [13]) on the surface of masonry elements and are primarily made of two

* Corresponding author.
E-mail addresses: matteo.canestri2@unibo.it (M. Canestri), francesca.ferretti10@unibo.it (F. Ferretti), claudio.mazzotti@unibo.it (C. Mazzotti).

https://doi.org/10.1016/j.jobe.2025.112072
Received 15 April 2024; Received in revised form 26 January 2025; Accepted 7 February 2025
Available online 8 February 2025

components: a mortar matrix, which may be lime- or cement-based, and a composite fibre textile made of various possible materials, such as carbon, Alkali-Resistant (AR) glass, aramid, basalt, steel or Poly-paraphenylene-benzo-bisoxazole (PBO).

The positive effects of these strengthening interventions were demonstrated and confirmed by several authors in a large number of studies [14–29], in which the in-plane or out-of-plane behaviour of masonry walls was analysed by means of experimental tests, with static or cyclic loading configurations. Moreover, the confinement effect provided by FRCM systems applied with single or multiple layers to masonry columns, according to different layout configurations, was also investigated with experimental and numerical analyses, proving the effectiveness of the strengthening solution [30–35].

Many real-world applications of these systems can be found on the exterior surfaces of buildings, with minimal protection from the potential effects of aggressive environments, such as freeze/thaw cycles, humidity, rainfall, and saline or alkaline attacks. For this reason, several recent experimental campaigns concentrated their efforts on studying the durability of these materials, especially when exposed to long-term environmental agents [36–40].

Another crucial aspect that is still being researched in the scientific literature is the residual efficiency of these retrofitting solutions after exposure to high temperature changes, such as those occurring in case of fire. The tensile behaviour of FRCM coupons reinforced with carbon fibres was studied at 200 °C and 400 °C [41], discovering that the behaviour of thermally conditioned uncoated carbon fibres could be improved by adding micro-steel and amorphous metallic fibres inside the mortar matrix. On the same typology of FRCM system, tensile tests were conducted at 200 °C, 300 °C and 400 °C and the impact of the number of fabric layers, thickness, and fibre orientation on the residual tensile behaviour was assessed [42]. Two separate experimental studies [43,44] were conducted to test the uniaxial tensile capacity of FRCM coupons reinforced with AR-glass at high temperatures. In the first study the influence of two distinct coating agents in the range 100–250 °C was investigated, while the effects of thermal cycles up to 600 °C on double layer configuration specimens were studied in the second work. The consequence of temperature exposure on the bond behaviour of FRCM systems reinforced with AR-Glass fibre was studied considering different bond lengths at three different temperature levels (100 °C, 200 °C and 300 °C); ultimately highlighting a shift in the obtained failure mode [45]. The possible introduction of a lightweight matrix, typically distinguished by a reduced thermal conductivity, was investigated in a subsequent study, with samples exposed to 120 °C and 200 °C [46]. The residual behaviour of FRCM systems made by basalt, glass, steel, PBO and carbon fibres applied on masonry wallets was investigated in three different experimental campaigns, in which single-lap direct shear tests were performed at different temperatures, all falling within the 100–500 °C range [47–49]. In two cases, a strong decrease in the obtained peak load was observed while increasing the temperature level for all materials, while the failure modes appeared to be less affected by the heating process. Conversely, the bond capacity was found to be compromised and a shift of failure mode was ultimately obtained at high temperatures in the most recent study [49].

Nonetheless, even if these retrofitting techniques are often placed on the outer surfaces of structural elements, only few studies focused on analysing the impacts of solar radiation approximately within the temperature range between 30 and 80 °C. An overall comparison of the tensile behaviour of FRCM systems reinforced with steel, basalt and aramid-glass fibres at 40 °C, 50 °C and 80 °C was presented in Ref. [50]. The outcomes demonstrated that the effects of temperature were mainly concentrated in the uncracked and cracks development phase of the tests, while the final stage, where the behaviour is controlled by the embedded fibres, was less affected. An investigation was conducted to examine the impact of two distinct surface treatments on the tensile behaviour of FRCM coupons reinforced with carbon fibres being exposed to a temperature of 50 °C and 98 % humidity [51]. The Authors investigated the effect of mild thermal exposure (between 32 °C up to 80 °C) on a FRCM system characterised by basalt fibres, applied to masonry wallets and subjected to single-lap direct shear tests: the effect of the temperature increase was evident on both the peak stress as well as on the obtained failure modes, which shifted from fibre failure to a complete fibre slippage inside the mortar layers [52]. The novelty of the testing setup used in Ref. [52] consisted in carrying out the single-lap direct shear tests inside the thermal chamber used to generate the detrimental environment. In fact, the majority of the available studies investigated the residual capacity by testing the specimens at room temperature, after their cooling down post thermal exposure.

The literature review provided, along with the few state-of-the-art reviews available on this critical subject [53–55], clearly emphasises the limited extension of current research in this field and identifies a significant knowledge gap that remains to be fully addressed. Additionally, the absence of a universally established testing protocol may obstruct meaningful comparisons of existing findings. For this reason, the development of a protocol is essential for standardizing research methodologies and enabling a more comprehensive assessment of the durability of these systems under temperature variations. In this research, the effect of mild temperature variations was studied on two FRCM systems, characterised by the use of reinforcing textiles made either with glass fibres only or by glass and aramid fibres. In a first step, the thermal conditioning was applied to the single components of the composite materials, thus investigating the thermal effects induced on their mechanical behaviour, i.e., tensile capacity for the dry textile; flexural and compressive strength for the mortar matrix. Subsequently, tensile tests and single-lap direct shear tests were also carried out on thermally conditioned FRCM coupons and FRCM-strengthened wallets, respectively. The paper aims to contribute to the data currently available on this topic, while providing an initial step toward the development of a standardised testing protocol.

2. Materials properties

2.1. Fibres

The FRCM systems examined in this study were made by two different types of reinforcing fibres. The first type (called *ARV* in the following) was a textile made of a composition of aramid and AR glass fibres, characterised by a weight density of 250 g/m^2 and featured two distinct equivalent thicknesses specified by the manufacturer: 0.031 mm in the warp direction and 0.049 mm in the weft direction. In more detail, in the warp direction, the bundles, 15 mm spaced, were composed alternatively by two yarns of glass fibres (*ARV_G*) and by one aramid and one glass yarn (*ARV_A*), as clearly illustrated in Fig. 1a. Instead, along the weft direction, a flat bundle made up of glass fibres was present, with a spacing equal to 18 mm. The yarns along the warp direction were wrapped around each other, while the yarns along the weft direction were simply incorporated into the weaving, without any kind of heat sealing. The second textile (named *ZR*) was composed of AR glass fibres evenly distributed in the two orthogonal directions (warp and weft), as illustrated in Fig. 1b. As declared by the manufacturer, the weight density was equal to 185 g/m^2, the bundle spacing was 16.5 mm, and the equivalent thickness was equal to 0.029 mm along both directions. The bundles oriented in the weft direction were slightly flatter and wider than those oriented in the warp direction; bundles in the warp direction were simply hot joined to the weft bundles without using any sort of mutual winding. Finally, an organic coating was applied to each individual yarn of both textiles, prior to the textile weaving process.

Tensile tests were carried out to characterise the mechanical features of the two textiles in the warp direction by using a servo-hydraulic testing machine, with a 100 kN maximum load capacity. A displacement control regime was used, with a constant velocity of 0.5 mm/min, according to the indications of the *Italian Guidelines for the identification, qualification and acceptance control of FRCM composites to be used for the structural strengthening of existing constructions* [56]. Averaged results between 2 tests are shown in Table 1 in terms of tensile strength ($\sigma_{u,f}$), ultimate strain ($\varepsilon_{u,f}$) and elastic modulus (E_f). For the ARV system, tensile tests were also conducted on bundle specimens (*ARV_A* and *ARV_G*), following the same Guidelines.

2.2. Mortar matrices

The two investigated fibre types are normally used for strengthening masonry elements in conjunction with lime-based mortar matrices. Two pre-mixed mortars were studied, one for each fibre type, both categorised by the producers as M15 according to the Standard EN 998–2:2016 [57]. Their mechanical properties were evaluated using standard testing methods from EN 1015–11:2020 [58]. The flexural strength was obtained from 40x40x160mm^3 specimens using the three-point bending test setup; afterwards, the compressive strength was evaluated from uniaxial compression tests on the prisms obtained from the flexural tests. After 28 days of curing in a controlled environment (T = 22 °C ± 1 °C, RH = 60 % ± 5 %), the mortar matrix related to the ARV system (named *NH1* in the following) was characterised by a density ρ_m = 1871 kg/m^3 (CoV 1.4 %), a flexural tensile strength $f_{m,fl}$ = 6.70 MPa (CoV 6.2 %) and a compressive strength $f_{m,c}$ = 20.21 MPa (CoV 4.1 %). For the mortar matrix of the ZR system (named *NH2* in the following), the density was equal to 1605 kg/m^3 (CoV 1.4 %), while the flexural tensile strength and the compressive strength were equal to 6.75 MPa (CoV 4.3 %) and 16.98 MPa (CoV 3.4 %), respectively.

2.3. Masonry substrate

The mechanical properties of the bricks and mortar adopted for the construction of the masonry wallets to be used for the single-lap direct shear tests were obtained through standard methods. Cylindrical samples, having diameter and height equal to 50 mm, were cored from the bricks: 12 samples were tested under uniaxial compression following the requirements imposed by EN 772–1:2011 Standard [59], while 12 samples were subjected to a Brazilian test, according to EN 12390–6:2009 Standard [60]. The obtained brick compressive strength $f_{b,c}$ was equal to 18.7 MPa (CoV 5.3 %), while the brick tensile strength ($f_{b,t}$) was 3.1 MPa (CoV 15.3 %). Three further samples, characterised by the same diameter and by a height of 125 mm, were subjected to cyclic compression tests (EN 12390–13:2013 [61]) for the determination of the brick elastic modulus (E_b) which resulted equal to 6.9 GPa (CoV 3.9 %). The mortar

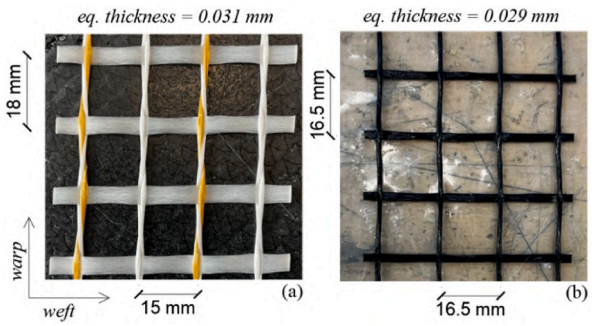

Fig. 1. Bundle spacing in warp and weft directions for the textiles: (a) ARV system, (b) and ZR system.

Table 1
Textile and bundle tensile properties at 23 °C.

Fibre type	Sample type	Tensile strength $\sigma_{u,f}$ (MPa)	Ultimate strain $\varepsilon_{u,f}$ (%)	Elastic modulus E_f (GPa)
ARV	Textile	2036	2.17	90.9
ARV_A	Bundle	2550	2.21	137.8
ARV_G	Bundle	1351	2.49	69.7
ZR	Textile	1202	1.69	83.3

underwent the same mechanical characterization procedure described in Section 2.2. A flexural strength ($f_{m,fl}$) equal to 1.5 MPa (CoV 15 %) and a compressive strength ($f_{m,c}$) equal to 4.8 MPa (CoV 12.5 %) were obtained.

3. Testing methods

In the present research, different types of specimens were manufactured and tested after being exposed to controlled thermal variations, following a specific conditioning protocol. The details of the manufacturing process for all these specimens, the thermal protocol employed, and the specifics of each test setup are described in this paragraph, while Fig. 2 provides a visual overview of the entire experimental campaign.

3.1. Specimen preparation

As previously introduced, tensile tests were performed on bundles, textiles and FRCM coupons, at different temperature levels. An overview of the geometrical dimensions of the samples is depicted in Fig. 3, where *s* is the thickness of the FRCM coupon and all the dimensions are specified in mm. Bundles were extracted for the ARV system only, while textile specimens were composed, for both FRCM systems, by four individual bundles along the warp direction. Textiles, having the same dimensions, were embedded between two 5-mm-thick mortar layers to manufacture FRCM coupons, following the suggestions of the RILEM TC 250-CSM [62]. An epoxy resin, capable of withstanding high-temperature variations after the polymerization process, was used to apply FRP tabs at both ends of all specimens with the aim of ensuring a homogeneous stress distribution between the individual bundles during the tensile test and avoiding local failures of the matrix in the FRCM coupons, caused by the pressure of the hydraulic grips of the testing machine.

Masonry prisms used for the single-lap direct shear specimens were manufactured by stacking 6 fired-clay bricks (120x250x55 mm^3), coupled together by 10 mm mortar joints. These masonry wallets were prepared and left curing inside a controlled environment for 28 days (T = 22 °C ± 1 °C, RH = 60 % ± 5 %) before being reinforced on one side with a composite strip, creating the standard single-lap direct shear specimen, with a bonded length equal to 300 mm for all specimens (Fig. 4). At the textile-to-matrix interface, the measuring tip of a thermocouple was embedded during the casting stage, with the aim of monitoring the temperature during all stages of the tests. The unbonded dry textile, 430 mm long, was impregnated with the same thermal resistant epoxy resin and strengthened with FRP tabs within the gripping area. It should be noted that the number of bundles included in the FRCM reinforcing strip was the same as the one adopted for tensile tests.

The specimens tested in this experimental campaign were identified by using the following notation: **XX_YY_AA_n**, where "XX" represented the tested material, i.e., either ARV or ZR, as previously mentioned; "YY" indicated the type of test: tensile test on textiles (TT), on bundles (BT) or on FRCM coupons (FT) and single-lap direct shear tests (DS). "AA" was the target temperature at which the tests were carried out, and "n" represented the specimen number.

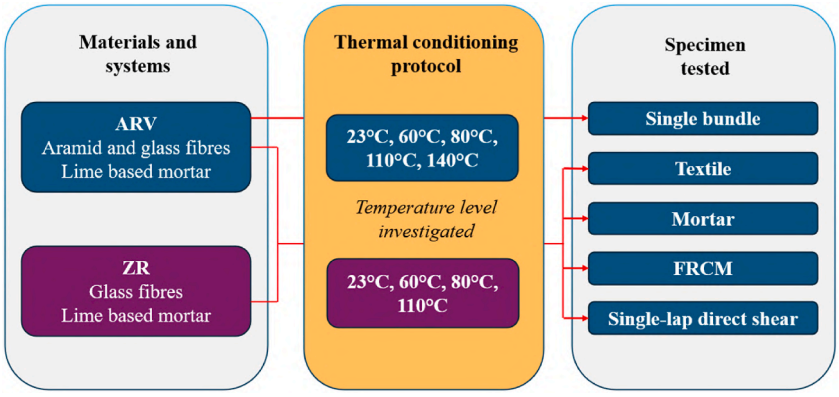

Fig. 2. Overview of the experimental campaign.

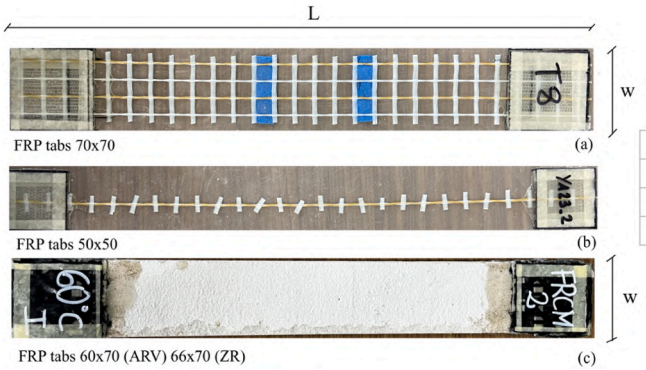

	ARV	ZR
L	500	500
w	60	66
s	10	10

Fig. 3. Geometrical dimensions (in mm) of: (a) textile, (b) bundle, (c) FRCM coupon.

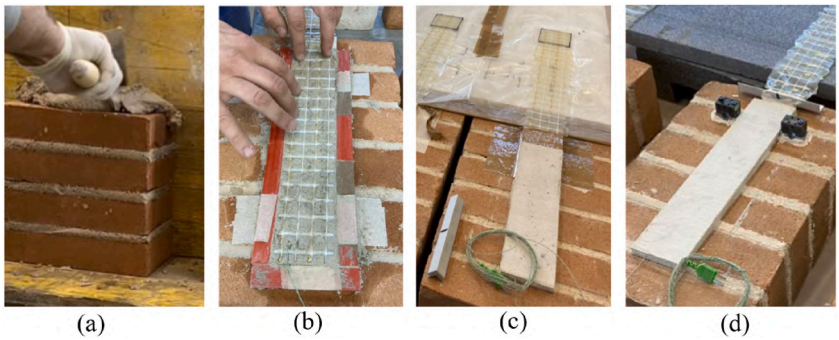

Fig. 4. Preparation of single-lap direct shear specimens: (a) construction of the wallets, (b) casting of the first mortar layer and positioning of the reinforcement, (c) impregnation of the unbonded textile with epoxy resin, (d) finished sample with thermocouple.

3.2. Thermal conditioning protocol

To apply a controlled thermal conditioning to the different specimens, a climatic chamber was used. This device enabled accurate regulation of the temperature level inside its enclosed space, within its operating working range of −129 °C and +315 °C. The temperature levels studied for the ARV system were 23, 60, 80, 110 and 140 °C, whereas the temperature levels explored for the ZR system were 23, 60, 80 and 110 °C. These conditioning environments were first applied to the constituents of the two FRCM systems for the evaluation of the tensile strength of the dry textile and bundle samples, together with the evaluation of the tensile and compressive strength of mortar matrix prisms. Subsequently, the tensile capacity of the FRCM systems was assessed through tensile tests on conditioned specimens, while their bond behaviour was studied through single-lap direct shear tests. All the tests were performed with the specimens inside the climatic chamber, with the goal of controlling the temperature level even during the test phases. In fact, the presence of the hydraulic grip inside the climatic chamber enabled testing at the required temperature without needing to open the door, thus preserving the continuity of the conditioning process. Furthermore, the heating process was not static, with an internal air circulation system activated to evenly distribute the heat. Preliminary experiments were conducted by placing a specimen inside the chamber, along with multiple thermocouples to measure the temperature at various points, confirming the uniformity of the heating process.

For the dry textile and bundle specimens, a constant heating gradient of 30 °C/h was imposed and the tests started when the target temperature (T_{target}), inside the thermal chamber, was reached. In fact, it is credible to consider that the temperature of the dry textile quickly increases as the temperature of the climatic chamber increases. Secondly, tests on mortar specimens were executed once the temperature at mid-height of the specimens reached 95 % of the target temperature, a K-type thermocouple sensor was embedded

Table 2
Thermal conditioning protocols for different specimens.

Specimen type	Heating rate (°C/h)	Exposure time definition (from the end of the heating phase)
Dry textile or single bundle	30	–
Mortar specimens	30	95 % of T_{target} is reached inside prisms
FRCM coupon	30	95 % of T_{target} is reached at interface mortar-textile
Single-lap direct shear test specimen	30	95 % of T_{target} is reached at interface mortar-textile

inside the mortar prisms and used to control the conditioning process. Subsequently, the conditioning process adopted for the FRCM coupons was chosen identical to the one adopted for the single-lap direct shear tests, since the thicknesses and widths of the composite were exactly the same. As far as the single-lap direct shear tests are concerned, a novel method proposed by the Authors in a previous experimental investigation [52] was here applied. In particular, a heating phase characterised by a constant gradient of 30 °C/h was initially imposed inside the thermal chamber, to reach the target temperature. Subsequently, a constant temperature phase started, whose duration was controlled by the reading of the K-type thermocouple installed at the textile-mortar interface. All the single-lap direct shear tests started as soon as the temperature registered by the thermocouple reached 95 % of the target one. The time elapsed between the start of the constant temperature phase and the beginning of the test was defined as *exposure time*, while the *total duration* included also the heating and the testing phases. Table 2 provides details of the heating rate and exposure time employed in the present study for the different specimen types.

3.3. Tensile test setup

The direct tensile tests were performed with a class 0.5 load cell-equipped servo-hydraulic testing machine with a 100 kN maximum load capacity. A displacement control regime with a constant velocity was imposed to all samples. In particular, following the prescription of the Italian Guidelines [56].

], tests on single bundle specimens and on dry textiles were conducted at 0.5 mm/min, while a variable velocity was assumed for the FRCM coupons: in the first uncracked phase, a speed of 0.2 mm/min was employed, which was then raised to 0.5 mm/min once the cracking phase was completed. The axial stress was obtained by dividing the registered load by the textile area for both specimen types. To measure the strain levels obtained during the testing phases, an extensometer, class 0.5 according to ISO 9513 [63], was applied in the middle of the specimens with a gauge length of 100 mm for the dry bundle and textile specimens and 200 mm for the FRCM coupons. An example of the adopted setup, for a FRCM textile and a coupon, is presented in Fig. 5.

3.4. Single-lap direct shear test setup

The bond tests of this experimental campaign were conducted with a single-lap direct shear configuration (Fig. 6), in accordance with the prescriptions of the Italian Guidelines [56] and the suggestions of the RILEM Technical Committee 250-CSM [62]. In this setup, the unbonded textile is pulled by the servo-hydraulic actuator of the testing machine, having the same characteristics described in Section 3.3, with a displacement rate of 0.2 mm/min. The masonry wallets were retained and held in place by a rigid steel frame, as shown in Fig. 6. The relative displacement between the unbonded textile and the substrate, named *global slip* in the following, was measured by two 20 mm Linear Variable Displacement Transducers (LVDT), fixed to the wallet and put in contact with an L-shaped aluminium plate, glued on the impregnated textile at the end of the bonded area.

When performing a single-lap direct shear test, different failure modes can be potentially obtained, depending on the characteristics of the substrate and the properties of the FRCM systems employed [64–66]: (i) debonding of the reinforcement strip with detachment of the substrate (DB), (ii) failure at the substrate-to-matrix interface (SM), (iii) complete rupture of the fibres just outside the bonded area (FR) or (iv) inside the composite strip (FM), (v) delamination at the textile-matrix interface (MT), (vi) complete slippage of the fibres within the mortar matrix (FS).

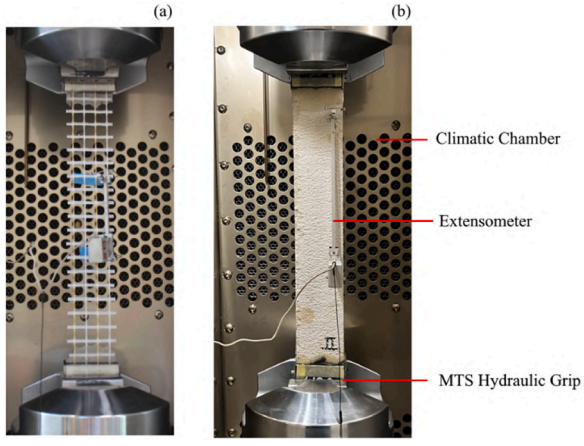

Fig. 5. Setup adopted for the direct tensile tests: (a) textile; (b) FRCM coupon.

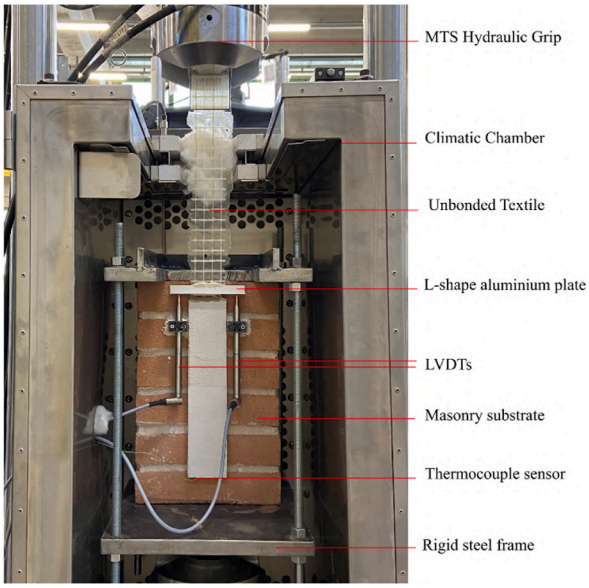

Fig. 6. Single-lap direct shear test setup.

4. Results

4.1. Aramid-glass FRCM system

4.1.1. Tensile tests on fibre bundles and textiles

For the ARV system, tensile tests were performed on bundle specimens composed by aramid and glass fibres yarns (A), on bundle specimens composed by glass fibers yarns only (G), and on aramid-glass textiles. The results of all the tests, 2 for each temperature level, are presented in Fig. 7.

Both glass (G) and aramid-glass (A) fibres bundle specimens showed an initial linear elastic stage followed by an irregular stage in which the two longitudinal yarns of the bundle unwound between one another, as depicted in Fig. 8. As a result, this phase was characterised by a plateau, in a deformation range approximately between 0.2 and 0.6 %. Subsequently, a hardening phase can be detected and, eventually, all tests reached the peak axial stress with a new linear elastic branch, characterized by a stiffness higher than that of the first branch. The elastic moduli reported in Table 3 were evaluated in this final stage. Textile specimens, instead, failed without any progressive untangling of the individual yarns, due to the stabilising effect offered by the fibres along the weft direction. They reached the tensile failure with a single linear elastic behaviour. In Table 3, the average results obtained in the tensile tests are provided for each temperature level examined, in terms of tensile strength ($\sigma_{u,f}$), elongation at failure ($\varepsilon_{u,f}$) and elastic modulus (E_f).

For each mechanical property, the Capacity Retention Rate (CRR) was assessed by using the following expression, in accordance with the instructions of the international standard ISO10406-1 [67]:

$$R_A = \left(\frac{A_T}{A_{T0}}\right) \bullet 100 \tag{1}$$

where A_T represents the general experimental property at a given temperature T and A_{T0} the corresponding property at ambient temperature ($T_0 = 23\ ^\circ C$), used as a reference.

The temperature exposure clearly affected the tensile capacity of both the individual bundles and the textiles, with a comparable trend in terms of capacity retention rates between the two types. Deformability and stiffness of the specimens were also affected by the thermal conditioning process, but with slightly higher retention rates compared to those characterising the tensile strength.

4.1.2. Flexural and compressive tests on mortars

In order to investigate the flexural and compressive strength of the mortar matrix adopted for the ARV system (NH1), a series of three-point bending tests and compression tests were carried out following the procedure reported in Section 2.2. A total of 25 mortar specimens were tested, 5 for each temperature level investigated. Average values of compressive strength ($f_{m,c}$) and flexural strength ($f_{m,fl}$) obtained from the tests are reported in Table 4, alongside the respective coefficients of variation (CoV in parenthesis).

Fig. 9 depicts the trend of the average compressive and flexural strengths against the target temperature of the tests, as well as the

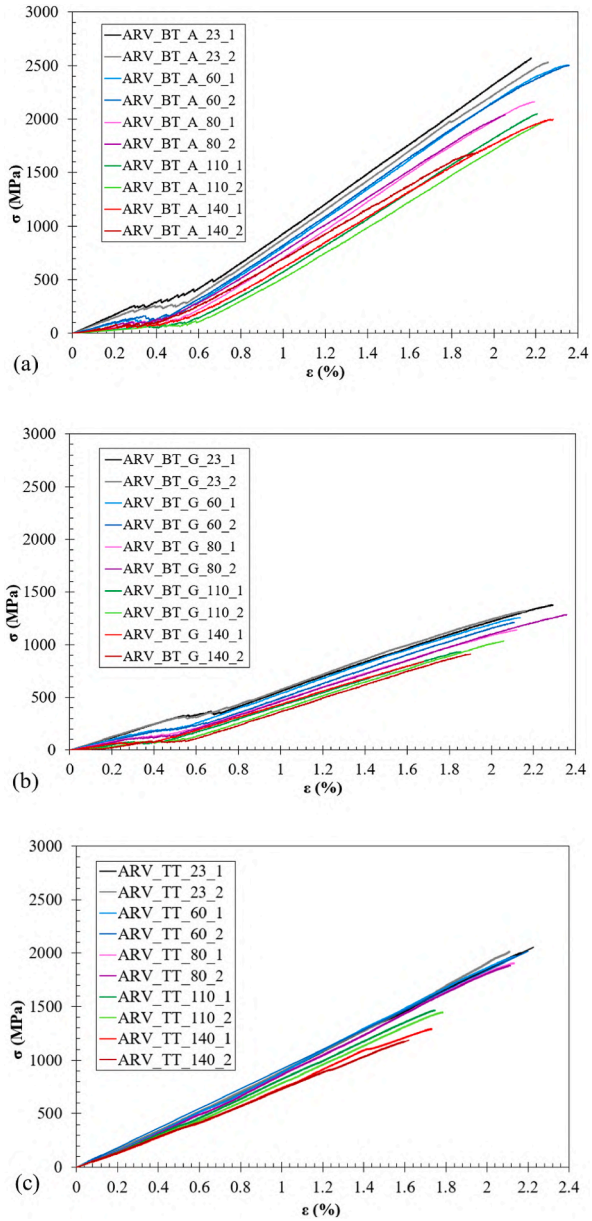

Fig. 7. ARV system: stress *vs* strain curves for tensile tests on bundle specimens (a, b) and textiles (c).

respective capacity retention rates. It can be noticed that a significant strength reduction was already obtained at 60 °C, whereas the reduction was essentially constant from 80 to 140 °C; this behaviour was observed for both compression and flexural test results.

Flexural and compressive tests were also conducted on the lime-based mortar used in the construction of the masonry wallets, which served as the substrate for the single-lap direct shear specimens. The effect of temperature in this case was negligible, with the CRR being 94 % for flexural strength and 97 % for compressive strength at the highest temperature level investigated (140 °C), values that fall within the range of statistical variation of the results.

4.1.3. Tensile tests on FRCM coupons

Tensile tests on FRCM coupons were performed following the test procedure described in Section 3.3, a total of 2 different tests for each temperature level. The stress *vs* strain curves are reported in Fig. 10. In Table 5, average axial stress (σ_u) and strain (ε_u) at failure are enlisted for each target temperature, together with the slope of the final branch (E_f) and their respective capacity retention rates.

The tensile strength of the FRCM coupons was already affected at 60 °C, with a residual capacity equal to 73 % of the reference one. The lowest value was reached for a target temperature equal to 110 °C, corresponding to 59 % of the strength of the samples tested at ambient temperature. The thermal conditioning had a lower impact on the deformability of the coupons, while the elastic modulus in

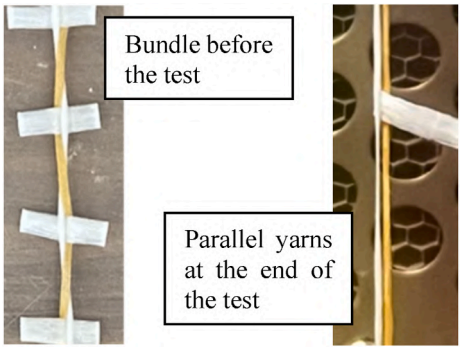

Fig. 8. Progressive unwinding of glass and aramid yarns (ARV_BT_A tests).

Table 3
ARV system: experimental results of the tensile tests on textile and bundle specimens.

Specimen type	Target temperature (°C)	Tensile strength		Ultimate strain		Elastic modulus	
		$\sigma_{u,f}$ (MPa)	CRR $\sigma_{u,f}$ (%)	$\varepsilon_{u,f}$ (%)	CRR $\varepsilon_{u,f}$ (%)	E_f (GPa)	CRR E_f (%)
BT_A	23	2550	100	2.22	100	135.4	100
	60	2504	98	2.36	106	134.2	99
	80	2100	82	2.12	96	127.5	94
	110	2009	79	2.21	99	119.3	88
	140	1840	72	2.10	94	110.3	81
BT_G	23	1351	100	2.23	100	75.9	100
	60	1233	91	2.12	95	68.2	90
	80	1213	89	2.24	101	64.7	85
	110	985	73	1.96	88	62.9	83
	140	876	65	1.79	80	61.6	81
TT	23	2036	100	2.17	100	90.9	100
	60	1993	98	2.17	100	90.3	99
	80	1896	93	2.12	98	84.9	93
	110	1458	72	1.77	81	82.6	91
	140	1239	61	1.68	77	73.8	81

Table 4
NH1 mortar: compressive and flexural strength at different target temperature.

Target temperature (°C)	Compressive strength		Flexural strength	
	$f_{m,c}$ (MPa)	CRR $f_{m,c}$ (%)	$f_{m,fl}$ (MPa)	CRR $f_{m,fl}$ (%)
23	20.21 (4.1 %)	100	6.70 (6.2 %)	100
60	17.68 (6.2 %)	87	3.61 (9.5 %)	54
80	15.36 (8.0 %)	76	3.00 (12.5 %)	45
110	16.60 (6.3 %)	82	3.62 (8.9 %)	54
140	15.74 (3.8 %)	78	3.26 (7.4 %)	49

the third stage was the property that was least affected, retaining 89 % of its capacity at a temperature of 140 °C. In comparison to the elastic modulus obtained for the dry fibre textiles (see Table 3), the values were slightly lower (90 %) at all temperature levels, except for a temperature of 140 °C, for which very similar values were registered.

4.1.4. Single-lap direct shear tests

In order to evaluate the bond behaviour of the ARV system applied to a masonry substrate, 2 single-lap direct shear tests were carried out at each temperature. The protocol that was implemented adhered to the indications provided in Section 3.2 and the acquisition of the temperature at the textile-mortar interface allowed to control the conditioning process. A recap of the exposure time and the total duration of the tests is presented in Table 6 for each target temperature studied.

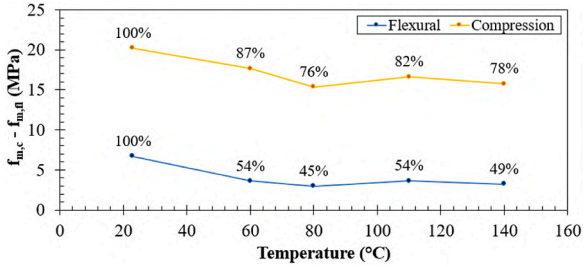

Fig. 9. NH1 mortar: flexural and compressive mortar strength *vs* temperature.

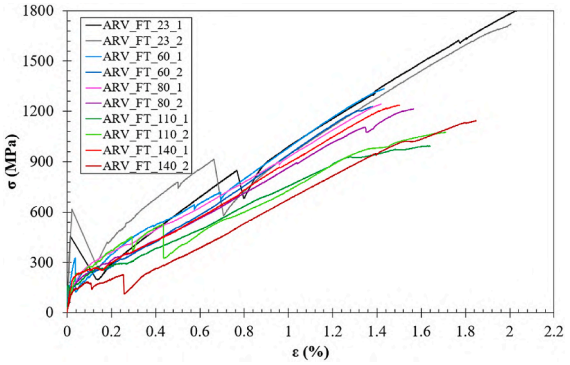

Fig. 10. ARV system: stress *vs* strain curves for tensile tests on FRCM coupons.

Fig. 11 shows the development of the conditioning process by comparing the imposed temperature inside the thermal chamber (dashed lines) with the thermocouple sensor readings (continuous lines). The heating process, inside the composite, was relatively fast in the initial hours of exposure, while it became noticeably slower as the hours passed, and it took a significant amount of time to asymptotically reach the chosen threshold, i.e., 95 % of the target temperature. The start (◆) and ending (▲) points of the tests are also reported in Fig. 11.

The experimental results of the single-lap direct shear tests are shown in Fig. 12 in terms of axial stress *vs* global slip curves, and data are reported in Table 7, in terms of peak load (F_b), peak axial stress (f_b), obtained failure mode and capacity retention rates. From Fig. 12, it can be noticed that a first linear elastic branch was obtained for all the investigated temperature levels. Subsequently, once a certain level of stress was reached, a decrease in stiffness was observed, more significant at lower temperatures, with minimal variation observed at 110 °C and 140 °C. This shift in deformability might be related to the onset of the debonding phenomena at the textile

Table 5
ARV system: experimental results of tensile tests on FRCM coupons.

Target temperature (°C)	Stress at failure		Strain at failure		Third stage elastic modulus	
	σ_u (MPa)	CRR σ_u (%)	ε_u (%)	CRR ε_u (%)	E_f (GPa)	CRR E_f (%)
23	1764	100	2.02	100	82.2	100
60	1281	73	1.41	70	80.3	98
80	1229	70	1.49	74	75.5	92
110	1035	59	1.67	83	72.2	88
140	1191	68	1.68	83	73.5	89

Table 6
ARV system: exposure time and total duration of the single-lap direct shear tests.

Target temperature (°C)	Exposure time (min)	Total duration (min)
23	–	20
60	315	420
80	340	500
110	280	500
140	400	700

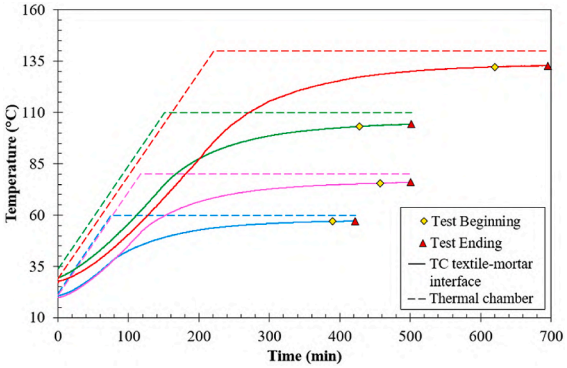

Fig. 11. ARV system: temperature profiles *vs* time in single-lap direct shear specimen at different target temperatures.

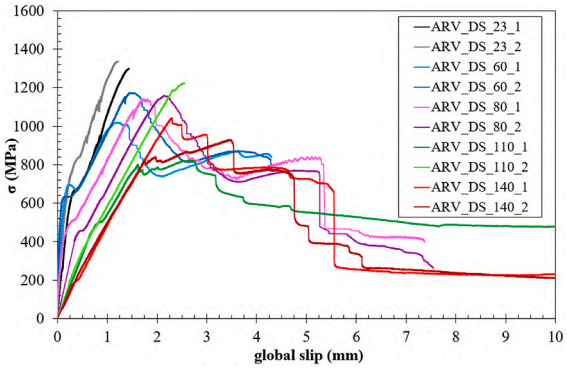

Fig. 12. ARV system: axial stress *vs* global slip curves.

mortar interface in the portion close to the loaded end. Subsequently, thanks to the interlocking mechanism between the longitudinal and the transversal bundles, an increase in stiffness was noticed up to the peak. Samples tested at 23 °C experienced a fragile failure after the peak, related to the tensile rupture of the fibres. Samples tested at a higher temperature, instead, were characterized by a drop in the load capacity and by a significant slip increase, corresponding to the propagation of the delamination. At this point, the stress values increased again for samples tested at 60 °C and 80 °C, probably due to the interlocking mechanism of the yarns and the mortar between the first and second transversal bundle. However, this mechanism seemed to be dependent on the effect of the temperature, since at high temperatures (at 110 °C and 140 °C), the stress increase was prevented and the delamination process continued after the peak, ultimately resulting in fibre slippage for some individual yarns and fibre breakage for others.

As far as the peak axial stresses were concerned, a reduction was already found at 60 °C, with a capacity retention rate equal to 83 %. By further increasing the temperature level up to 140 °C, an additional capacity reduction was observed but limited to a total of 8 %, indicating a reducing effect of further temperature increase.

A representation of the two main failure modes obtained in the tests is shown in Fig. 13: the entire reinforcement strip is shown at

Table 7
ARV system: single-lap direct shear test results.

ID	Target Temperature (°C)	Peak Load		Peak Axial Stress			
		F_b (kN)	Average (kN)	f_b (MPa)	Average (MPa)	CRR f_b (%)	Failure Mode
DS_23_1	23	2.42	2.45	1299	1317	100	FR
DS_23_2	23	2.48		1336			FR
DS_60_1	60	1.90	2.04	1020	1096	83	FR
DS_60_2	60	2.18		1173			FR
DS_80_1	80	2.12	2.14	1142	1151	87	FR
DS_80_2	80	2.16		1159			FR
DS_110_1	110	1.53	1.90	822	1023	78	FS-FR[a]
DS_110_2	110	2.28		1224			FR
DS_140_1	140	1.94	1.83	1042	987	75	FS-FR[a]
DS_140_2	140	1.73		931			FS-FR[a]

[a] Mixed failure mode.

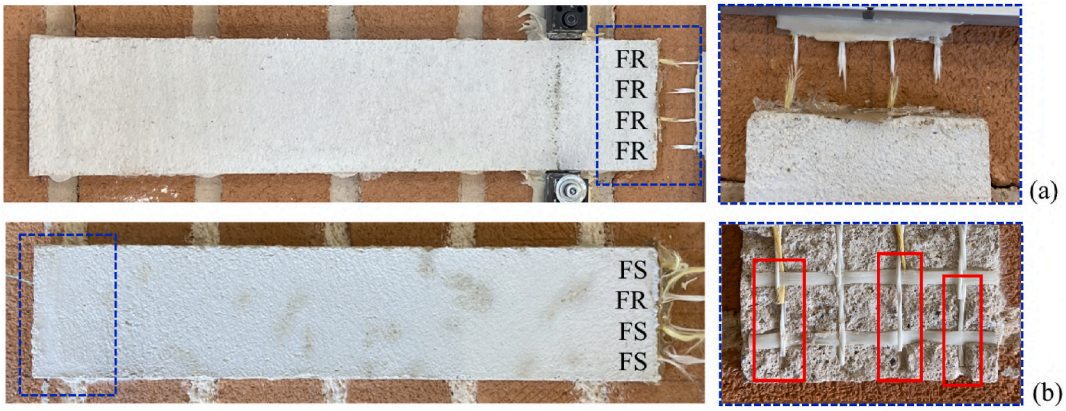

Fig. 13. ARV system: characteristic failure modes in single-lap direct shear tests (a) fibre rupture (DS_23_1), (b) mixed failure mode (DS_110_1).

failure, alongside magnified details of the failure zone. For samples tested at 23, 60 and 80 °C, the fibres failure was observed just outside the bonded area (Fig. 13a). Conversely, for samples tested at 110 and 140 °C, some individual yarns started to slip within the mortar. To prove this, the first layer of mortar was gently removed showing some displaced yarns at the end of the bonded strip, as can be observed in Fig. 13b. However, only some aramid and glass cords started to slip, without involving the full bundles, thus leading to a mixed failure mode.

4.2. Glass FRCM system

4.2.1. Tensile tests on fibre textiles

The constitutive behaviour of the dry fibre textiles, expressed in terms of stress *vs* strain curves for all the investigated temperature levels, obtained from two individual tests, is reported in Fig. 14. The peak failure load was obtained in all the tests after an initial linear elastic branch, which then became slightly non-linear when approaching the rupture.

In Table 8, the average values of the maximum tensile strength ($\sigma_{u,f}$), ultimate strain ($\varepsilon_{u,f}$) and modulus of elasticity (E_f) are reported for each temperature level investigated. For all the mechanical properties, their respective capacity retention rates were evaluated and reported.

A detrimental effect given by the temperature exposure on the tensile capacity was observed, with a capacity retention rate as low as 69 % for the 110 °C specimens. A similar effect was also observed on the ultimate strain and on the elastic modulus of the material, even if the latter was characterized by higher retention rates, compared to those characterising the tensile strength.

4.2.2. Flexural and compressive tests on mortars

A total of 16 mortar prisms were tested for the mortar associated with the ZR system (NH2), 4 for each temperature level investigated. In Table 9, average values of compressive strength ($f_{m,c}$) and flexural strength ($f_{m,fl}$) are listed, alongside their respective coefficients of variation (in parenthesis).

Fig. 15 shows the relationship between the mortar strengths, i.e. compression and flexural, and the target temperature as well as the corresponding capacity retention rates. In comparison with the mortar of the ARV system, flexural and compression capacity were less affected by the temperature increase, with retention rates reaching 80 % only at 110 °C in the flexural tests.

As previously noted in Section 4.1.2, the compressive and flexural strength of the mortar used to build the masonry wallets was evaluated, revealing that temperature had a negligible influence on its properties.

4.2.3. Tensile tests on FRCM coupons

Tensile tests on FRCM coupons, 2 for each temperature level, were performed following the indications provided in Section 3.3, and the results are reported in Fig. 16 in terms of stress *vs* strain curves. In Table 10, values of stress and strain at failure were reported (σ_u, ε_u) alongside stiffness of the final branch of the curve (E_f). For these mechanical properties, capacity retention rates were also evaluated and reported.

A progressive impact on the tensile strength of the FRCM coupons was observed by increasing the target temperature, reaching a capacity retention rate equal to 63 % for the specimens tested at 110 °C. A strong reduction was also observed in terms of deformation at failure, which reached 63 % of ε_u at reference temperature at the highest temperature investigated. However, it was observed that

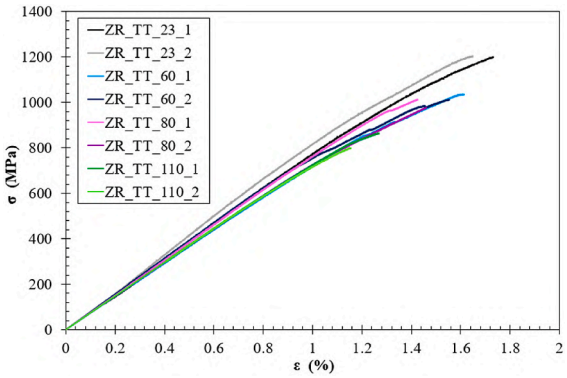

Fig. 14. ZR system: experimental stress *vs* strain curves on textile specimens.

the stiffness of the third branch was seemingly not affected by the heating treatment, conversely to the elastic modulus obtained on dry fibre textiles (Table 8). This result could be potentially explained by the positive shielding effect provided by the mortar layers, which resulted in being only slightly affected by the thermal exposure (Fig. 15).

4.2.4. Single-lap direct shear tests

In order to carry out the single-lap direct shear tests, the conditioning procedure described in Section 3.2 was used and the results in terms of exposure times and total duration of the tests are presented in Table 11.

Fig. 17 shows the temperature profiles inside both the environmental chamber (dotted line) and at the interface (continuous line) between the two components of the composite materials, obtained from the embedded thermocouple sensor. As can be deduced from

Table 8
ZR system: experimental results on textile specimen.

Target temperature (°C)	Tensile strength		Ultimate strain		Elastic modulus	
	$\sigma_{u,f}$ (MPa)	CRR $\sigma_{u,f}$ (%)	$\varepsilon_{u,f}$ (%)	CRR $\varepsilon_{u,f}$ (%)	E_f (GPa)	CRR E_f (%)
23	1202	100	1.69	100	83.3	100
60	1024	85	1.58	94	74.8	90
80	995	83	1.44	85	73.8	89
110	832	69	1.21	72	69.9	84

Table 9
NH2 mortar: compressive and flexural strength of the mortar at different target temperature.

Target temperature (°C)	Compressive strength		Flexural strength	
	$f_{m,c}$ (MPa)	CRR $f_{m,c}$ (%)	$f_{m,fl}$ (MPa)	CRR $f_{m,fl}$ (%)
23	16.98 (3.4 %)	100	6.75 (4.3 %)	100
60	16.52 (8.5 %)	97	5.87 (4.3 %)	87
80	16.17 (5.9 %)	95	5.52 (0.9 %)	82
110	15.61 (6.4 %)	92	5.37 (5.9 %)	80

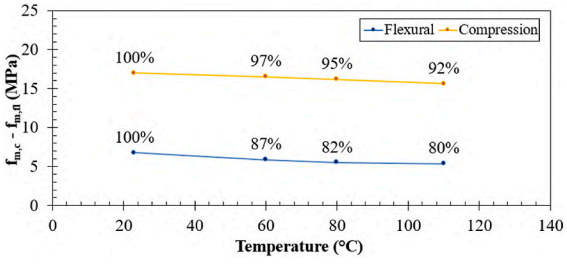

Fig. 15. NH2 mortar: flexural and compression mortar strength *vs* temperature.

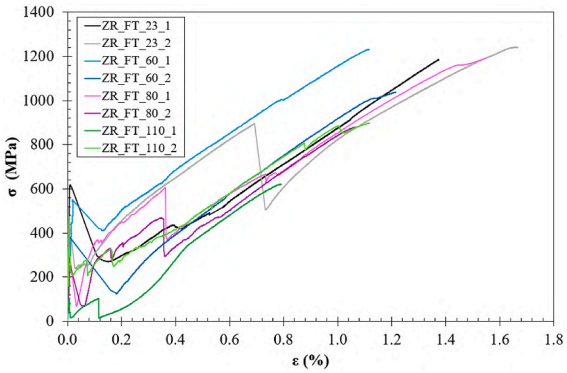

Fig. 16. ZR system: experimental stress *vs* strain curves on FRCM coupons.

Table 10
ZR system: experimental results on FRCM coupons.

Target temperature (°C)	Stress at failure		Strain at failure		Third stage elastic modulus	
	σ_u (MPa)	CRR σ_u (%)	ε_u (%)	CRR ε_u (%)	E_f (GPa)	CRR E_f (%)
23	1214	100	1.52	100	83.7	100
60	1135	93	1.17	77	83.2	99
80	1036	85	1.31	86	84.4	101
110	760	63	0.95	63	84.7	101

the curves, the heating process in the composite was initially rapid, but gradually slowed down over time, eventually taking a considerable length of time to approach the specified threshold.

The experimental curves, expressed in terms of axial stress *vs* global slip, are reported in Fig. 18, for each investigated temperature level. Additionally, in Table 12, values of peak load (F_b), peak axial stress (f_b) and obtained failure mode are reported, alongside their respective capacity retention rates.

From the obtained experimental results, the stiffness of the samples was clearly affected and influenced by the temperature variations. Tests carried out at 23 °C and 60 °C showed a linear elastic behaviour followed by a slightly nonlinear phase until failure point was reached. Conversely, in the 80 °C and 110 °C specimens, a stiffness decrease was observed once a certain level of stress was reached, attributable to the progressive propagation of the delamination phenomena at the textile-mortar interface, with a mechanism similar to what was observed for the ARV system; however, no stress drop was recorded at 80 °C and failure occurred for fibre rupture outside the bonded area. For samples tested at 110 °C, the effect of temperature led to a global behaviour characterised by a progressively increasing slip at an almost constant value of stress. Concerning the bond strength at the different temperatures, a significant decrease was obtained when increasing the temperature level, as can be seen in Table 12.

An example of the two main failure modes obtained with the ZR system is reported in Fig. 19, with an overview of the whole reinforcement strip and a detailed view of the bonded area. At 23, 60 and 80 °C, a tensile failure occurred in the textile just outside the loaded end of the reinforcement strip (Fig. 19a). However, at 110 °C a shift in the failure mode was observed, ultimately leading to a complete slippage of the fibre bundles inside the reinforcement strip (Fig. 19b). In fact, the weak connection between the two main directions of the textile, as previously described, was much affected by the temperature variation and the simple heat-sealing connection between the two was easily lost at 110 °C. Moreover, organic components inside the coating applied to the fibres, further weakened the interface between the two materials when exposed at high temperatures.

5. Comparison and discussion

To study the effect of temperature variations on the mechanical behaviour of FRCM systems, a comparison was made between the results of the tests on the dry textiles, on the FRCM coupons, and on the single-lap direct shear specimens. To enhance the comparison,

Table 11
ZR system: exposure time and total duration of the single-lap direct shear tests.

Target temperature (°C)	Exposure time (min)	Total duration (min)
23	–	30
60	295	400
80	345	520
110	470	680

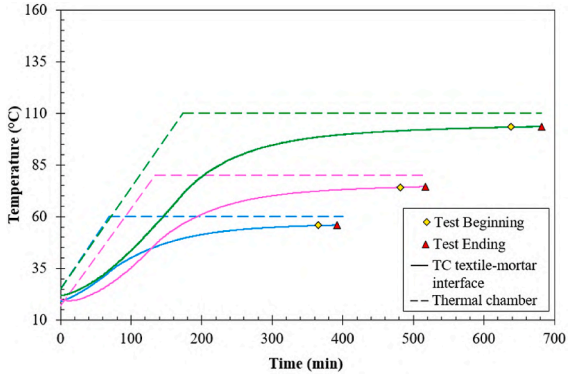

Fig. 17. ZR system: temperature profiles *vs* time in single-lap direct shear specimen at different target temperatures.

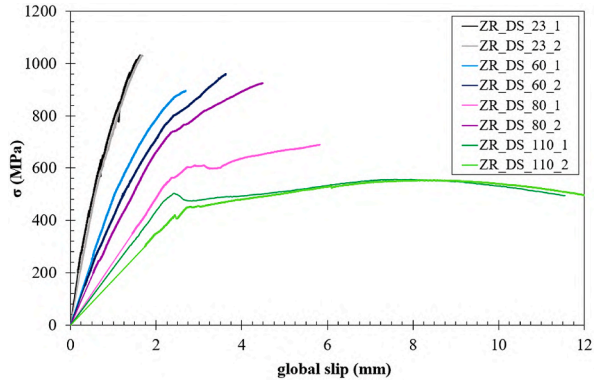

Fig. 18. ZR system: axial stress *vs* global slip curves.

expressed in terms of average peak axial stress *vs* temperature level, the results obtained by the Authors on an additional FRCM system (named B2 in the following) are also considered. The B2 system was characterised by a balanced basalt textile with a weight density of 210 g/m^2, an equivalent thickness of 0.034 mm and a bundle spacing of 16 mm. The matrix adopted for the composite material was the same lime-based mortar used for the ZR system and whose results in terms of compression and flexural strength are reported in Section 4.2.2. In a previous experimental campaign [52], a series of single-lap direct shear tests were performed, at different temperature levels, while in the present work, to provide an exhaustive comparison, additional tests were conducted on the B2 system: dry fibre textiles and FRCM coupons were subject to tensile tests at four different temperature levels: 23, 40, 50 and 80 °C, consistent with the target temperatures already examined in the single-lap direct shear tests [52].

In Fig. 20, the comparisons in terms of average tensile strength *vs* temperature are shown off for the three analysed systems. In particular, a trend line was added for each sample type (textile, FRCM coupons or single-lap direct shear specimens), in order to describe the capacity decay with the temperature increase. The highest value of the coefficient of determination R^2 was used as the criteria to choose the best possible approximation of the experimental findings. As a result, all experimental data were best approximated by exponential functions, whose equations are reported in Fig. 20 as well. In more details, for the ARV system (Fig. 20a), tests on textile specimens revealed a more significant influence of temperature when it exceeded 60 °C. In contrast, the impact of the temperature exposure on the tensile capacity of the FRCM coupons and on the single-lap direct shear test results was generally less

Table 12
ZR system: single-lap direct shear test results.

ID	Target Temperature (°C)	Peak Load		Peak Axial Stress			
		F_b (kN)	Average (kN)	f_b (MPa)	Average (MPa)	CRR f_b (%)	Failure Mode
DS_23_1	23	1.96	1.96	1031	1029	100	FR
DS_23_2	23	1.95		1026			FR
DS_60_1	60	1.70	1.77	897	929	90	FR
DS_60_2	60	1.83		961			FR
DS_80_1	80	1.31	1.54	690	808	78	FR
DS_80_2	80	1.76		925			FR
DS_110_1	110	1.06	1.06	557	556	54	FS
DS_110_2	110	1.05		555			FS

pronounced and followed a similar trend, as indicated by the exponential curves. On the other hand, the results on the ZR system (Fig. 20b) clearly demonstrated that all types of tests exhibited a similar decay trend. Finally, the results on textiles and FRCM coupons of the B2 system (Fig. 20c) exhibited a similar exponential decay, while the results of the single-lap direct shear tests highlighted a much stronger effect of the temperature increase on the bond strength, ultimately leading to a very low value in correspondence with 80 °C. For all the materials, a great effect induced by the thermal variations was registered, as demonstrated by the decreasing trends obtained for all the test typologies. In general, it can be observed that, for the investigated temperature levels, the highest stress values were registered for the tensile tests conducted on dry fibres, while lower values were obtained from the FRCM coupons, probably due to the different stress redistribution among the fibre bundles due to the presence of the mortar matrix. In all instances, the lowest results were the ones observed in the single-lap direct shear tests, as expected due to the change in terms of failure modes, as previously discussed.

Lastly, a comparison between the capacity retention rates for the investigated temperature levels was carried out comparing tests on textile (Fig. 21a), FRCM coupons (Fig. 21b) and single-lap direct shear tests (Fig. 21c) for the three systems. The inclusion of linear trendlines in the graphs allows to observe that, for textile and FRCM coupon tests, a similar adverse effect of temperature exposure could be observed for all the systems. However, significant disparities in these trendlines were observed in the single-lap direct shear tests. More specifically, the steeper the slope of the trendline, the more significant the change, at each target temperature, from a failure mode with fibre rupture with minimal slippage to complete fibre slippage.

6. Conclusions

In this experimental work, the mechanical behaviour of FRCM systems after controlled thermal exposure was thoroughly analysed at different scales. In fact, tests were carried out on thermally conditioned mortar prisms, textile and bundle specimens, FRCM coupons and single-lap direct shear test samples. Two different FRCM systems were studied, both characterised by natural lime-based matrices and by a glass-only or a glass-aramid fibre textile. They were tested inside a climatic chamber at different target temperatures, ranging from 23 °C up to 140 °C, and the testing procedures were specifically defined, e.g. the exposure time was established thanks to the reading of a thermocouple embedded at the textile-mortar interface in the single-lap shear test specimens. The study revealed that thermal exposure significantly impacts both tensile and bond capacity, highlighting critical changes in the behaviour of the constituent materials—fibers, coatings, and mortar matrices—when subjected to thermal variations.

In terms of tensile properties of bundle and textile specimens, a marked decline in mechanical properties was observed with increasing temperature for both ARV and ZR systems. More specifically, looking at the textile properties, a Capacity Retention Rate (CRR) equal to 61 % was obtained for the ARV system at 140 °C, while a CRR of 69 % at 110 °C was found for the ZR system. These reductions can be attributed to thermally induced degradation of the fibers and, especially, of the coatings. Indeed, the organic coating applied to the textiles plays a critical role in stress transfer between fibers, but its thermal sensitivity could lead to a decay of the properties at high temperatures, resulting in reduced adhesion, compromising the tensile capacity and, to a lower extent, the stiffness of the textiles.

FRCM coupons exhibited similar trends. In the ARV system, tensile strength retention rates were equal to 73 % at 60 °C and reached 59 % at 110 °C, reflecting the combined effects of matrix degradation and thermal deterioration of the textile. The ZR system displayed a more gradual reduction, with a tensile strength CRR of 63 % at 110 °C, likely due to the relatively lower thermal sensitivity of its mortar matrix. However, the elastic modulus in the cracked stage of the tests for both systems demonstrated greater resilience, maintaining over 89 % of its initial value at 140 °C for ARV and close to 100 % for ZR at 110 °C. These results confirmed that the tensile strength is more susceptible than the elastic modulus to a decay with increasing temperature.

In single-lap direct shear tests, both systems exhibited a pronounced temperature-dependent decrease in bond strength. The ARV system showed a CRR of 75 % at 140 °C, while the ZR system demonstrated a sharper decline, with a CRR of only 54 % at 110 °C. This

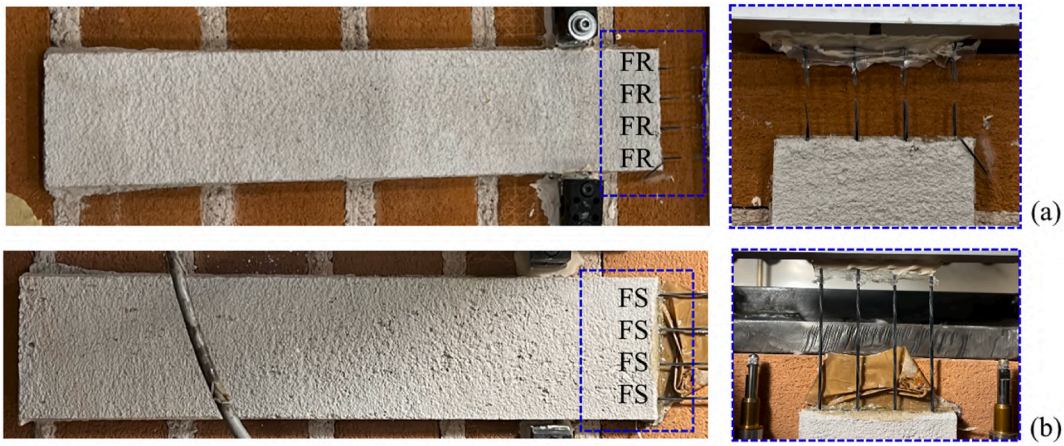

Fig. 19. ZR system: characteristic failure modes: (a) fibre rupture (DS_23_2), (b) fibre slippage (DS_110_1).

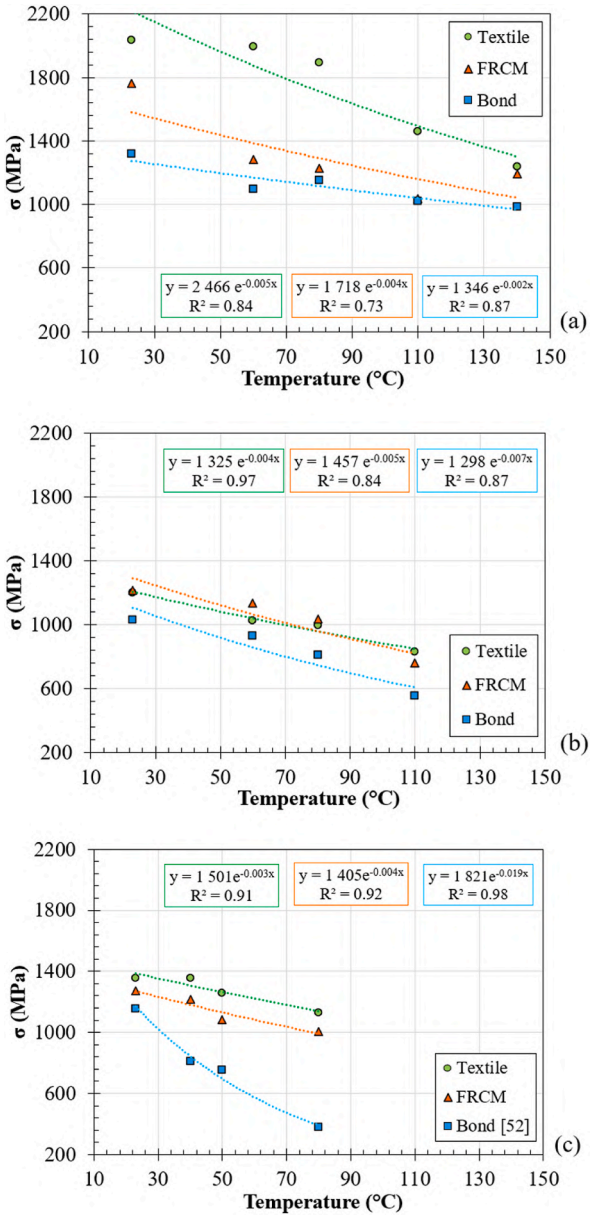

Fig. 20. Peak axial stress *vs* temperature from each sample type: textile, FRCM and single-lap direct shear specimens: (a) ARV system, (b) ZR system, (c) B2 system.

disparity can be attributed to the heat-sealed connections between the warp and weft bundles for the ZR system, which were more susceptible to detachment at elevated temperatures. The ARV system, by contrast, benefitted from enhanced interlocking effect of its textile configuration. Moreover, the failure modes shifted with increasing temperature: the ARV system transitioned from fibre rupture at lower temperatures to mixed failure (partial fibre slippage combined with rupture) at higher temperatures. In contrast, the ZR system exhibited a complete shift from fibre rupture to fibre slippage within the matrix at 110 °C, highlighting the critical role of the coating and bundle integrity in the bond behaviour.

This study highlighted the critical role of thermal exposure in altering the mechanical performance and failure mode of two glass-based FRCM composite systems. The thermal degradation of the textile, coatings, and mortar matrices determined a reduction of the tensile capacity and a negative impact on the bond performance on masonry substrates. Organic coatings, essential for stress transfer and fibre protection, were particularly vulnerable to thermal exposure, leading to slippage and a reduction in tensile capacity. Furthermore, the connection between the orthogonal bundles of the textiles played a crucial role: poor connections due to insufficient mutual winding could trigger an early bond failure and potentially make the composite more susceptible to prolonged temperature exposure.

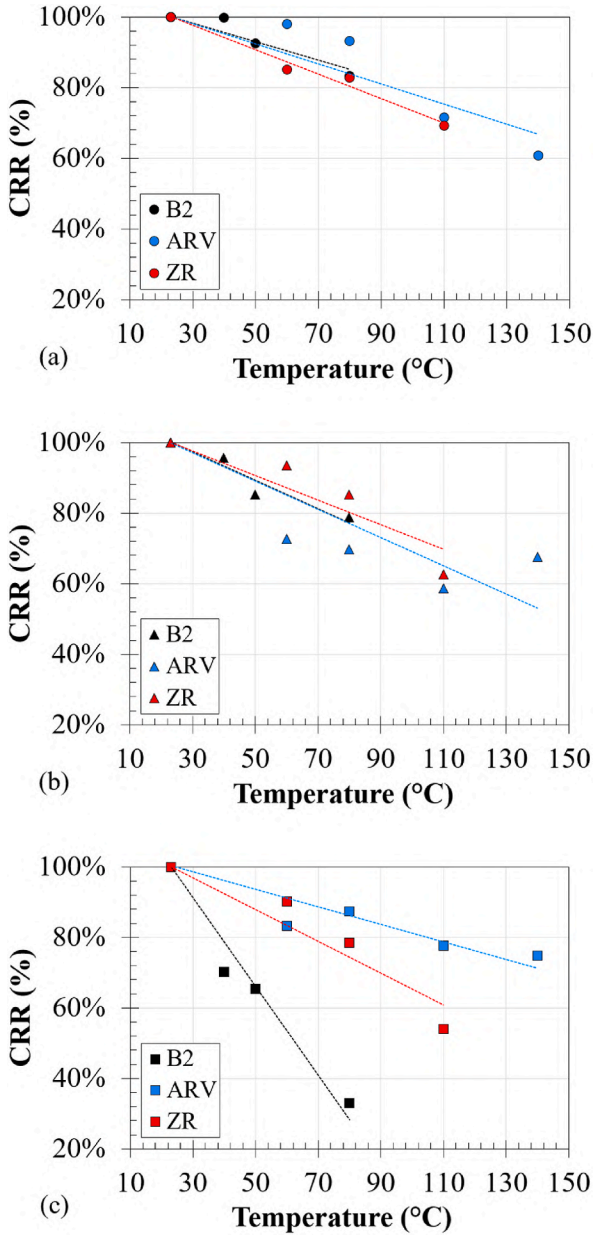

Fig. 21. Capacity retention rates *vs* temperature across different sample type: (a) textile, (b) FRCM coupons, (c) single-lap direct shear wallets.

The findings offer valuable insights into the effects of mild thermal exposure on FRCM systems, emphasising the need for standardised testing protocols to advance research and enable comparisons across studies. In the experimental campaign, the proposed protocol was applied to ensure the composite reached a specific temperature before the beginning of the test, without analysing variations in terms of heating rate, which was chosen according to Standards recommendations [56]. The transition in failure modes under higher temperatures was closely linked to the properties of the organic coating and textile design; therefore, variations in the chemical and physical properties of the coatings could still be explored, leaving room for further research. In general, caution is needed when generalising these results to other glass, aramid and basalt fibres-based FRCM systems, as variations in coatings and mortar properties across different systems might yield diverse outcomes.

CRediT authorship contribution statement

Matteo Canestri: Writing – original draft, Visualization, Methodology, Investigation, Formal analysis. **Francesca Ferretti:** Writing – review & editing, Supervision, Methodology, Conceptualization. **Claudio Mazzotti:** Writing – review & editing, Supervision,

Funding acquisition, Conceptualization.

Declaration of competing interest

The authors declare that they have no known competing financial interests or personal relationships that could have appeared to influence the work reported in this paper.

Acknowledgments

The financial support of the Italian Department of Civil Protection (ReLUIS 2024–2026 Grant-WP14) is gratefully acknowledged. Andrea Incerti and Anna Rosa Tilocca (Technical staff at CIRI Buildings & Construction), together with the master students Antonella Morganti and Francesca Nanni, are gratefully acknowledged for their work on the experimental tests.

Data availability

Data will be made available on request.

References

[1] M.G. D'Urso, C.L. Marino, J. Aldrighettoni, Degradation of historic masonry by analytical and digital photogrammetry: a quantitative analysis. ISPRS annals of the photogrammetry, Rem. Sens. Spat. Inform. Sci. X-M-1–2023 (2023, June 23) 47–54, https://doi.org/10.5194/isprs-annals-x-m-1-2023-47-2023.
[2] A. De Stefano, E. Matta, P. Clemente, Structural health monitoring of historical heritage in Italy: some relevant experiences, J. Civ. Struct Health Monitor. 6 (1) (2016, February) 83–106, https://doi.org/10.1007/s13349-016-0154-y.
[3] S. Baraccani, A. Piccolo, G. Gasparini, M. Palermo, T. Trombetti, AN assessment of the structural behaviour of the GARISENDA tower in bologna through finite element modelling and structural health monitoring. Proceedings of the 7th International Conference on Computational Methods in Structural Dynamics and Earthquake Engineering (COMPDYN 2015), 2019, https://doi.org/10.7712/120119.7314.19061.
[4] G. Leoni, A. Zona, Q. Piattoni, A. Meschini, E. Petrucci, A. Dall'Asta, L. Dezi, Assessment of seismic vulnerability of historical defensive walls. Proceedings of the 5th International Conference on Computational Methods in Structural Dynamics and Earthquake Engineering (COMPDYN 2015), 2015, https://doi.org/10.7712/120115.3506.771.
[5] F. Micelli, A. Cascardi, S. Verre, Structural assessment of a heritage building in the UNESCO site of alberobello, Lect. Notes Networks Syst. (2022) 2203–2212, https://doi.org/10.1007/978-3-031-06825-6_212.
[6] A. Penna, C. Calderini, L. Sorrentino, C.F. Carocci, E. Cescatti, R. Sisti, A. Borri, C. Modena, A. Prota, Damage to churches in the 2016 central Italy earthquakes, Bull. Earthq. Eng. 17 (10) (2019, March 16) 5763–5790, https://doi.org/10.1007/s10518-019-00594-4.
[7] E. Curti, S. Podestà, S. Resemini, The post-earthquake reconstruction process of monumental masonry buildings: suggestions from the molise event (Italy), Int. J. Architect. Herit. 2 (2) (2008, May 22) 120–154, https://doi.org/10.1080/15583050701646703.
[8] P. Foraboschi, Effectiveness of novel methods to increase the FRP-masonry bond capacity, Compos. B Eng. 107 (2016, December) 214–232, https://doi.org/10.1016/j.compositesb.2016.09.060.
[9] C. Mazzotti, F. Murgo, Numerical and experimental study of GFRP-masonry interface behavior: bond evolution and role of the mortar layers, Compos. B Eng. 75 (2015, June) 212–225, https://doi.org/10.1016/j.compositesb.2015.01.034.
[10] C. Carloni, K.V. Subramaniam, FRP-masonry debonding: numerical and experimental study of the role of mortar joints, J. Compos. Construct. 16 (5) (2012, October) 581–589, https://doi.org/10.1061/(asce)cc.1943-5614.0000282.
[11] E. Sassoni, S. Andreotti, A. Bellini, B. Mazzanti, M.C. Bignozzi, C. Mazzotti, E. Franzoni, Influence of mechanical properties, anisotropy, surface roughness and porosity of brick on FRP debonding force, Compos. B Eng. 108 (2017, January) 257–269, https://doi.org/10.1016/j.compositesb.2016.10.020.
[12] P. Carrara, D. Ferretti, F. Freddi, Debonding behavior of ancient masonry elements strengthened with CFRP sheets, Compos. B Eng. 45 (1) (2013, February) 800–810, https://doi.org/10.1016/j.compositesb.2012.04.029.
[13] Consiglio nazionale delle ricerche, Guide for the Design and Construction of Externally Bonded Fibre Reinforced Inorganic Matrix Systems for Strengthening Existing Structures, National Research Council, CNR, Rome, Italy, 2018. CNR-DT 215/2018.
[14] M. Santandrea, F. Focacci, C. Mazzotti, F. Ubertini, C. Carloni, Determination of the interfacial cohesive material law for SRG composites bonded to a masonry substrate, Eng. Fail. Anal. 111 (2020, April) 104322, https://doi.org/10.1016/j.engfailanal.2019.104322.
[15] E. Sassoni, C. Mazzotti, G. Pagliai, Comparison between experimental methods for evaluating the compressive strength of existing masonry buildings, Constr. Build. Mater. 68 (2014, October) 206–219, https://doi.org/10.1016/j.conbuildmat.2014.06.070.
[16] F.S. Murgo, F. Ferretti, C. Mazzotti, A discrete-cracking numerical model for the in-plane behavior of FRCM strengthened masonry panels, Bull. Earthq. Eng. 19 (11) (2021, May 28) 4471–4502, https://doi.org/10.1007/s10518-021-01129-6.
[17] F. Ferretti, A. Incerti, A.R. Tilocca, C. Mazzotti, In-plane shear behavior of stone masonry panels strengthened through grout injection and fiber reinforced cementitious matrices, Int. J. Architect. Herit. 15 (10) (2019, October 9) 1375–1394, https://doi.org/10.1080/15583058.2019.1675803.
[18] L. Garcia-Ramonda, L. Pelà, P. Roca, G. Camata, Experimental and numerical analysis of the cyclic in-plane behaviour of retrofitted masonry walls, 9th Euro-Am. Congr. Construct. Pathol. Rehabilit. Technol. Heritag. Manag. (REHABEND) (2022, September) 1962–1970.
[19] L. Garcia-Ramonda, L. Pelà, P. Roca, G. Camata, Cyclic shear-compression testing of brick masonry walls repaired and retrofitted with basalt textile reinforced mortar, Compos. Struct. 283 (2022, March) 115068, https://doi.org/10.1016/j.compstruct.2021.115068.
[20] L. Garcia-Ramonda, L. Pelà, P. Roca, G. Camata, Experimental cyclic behaviour of shear masonry walls reinforced with single and double layered Steel Reinforced Grout, Constr. Build. Mater. 320 (2022, February) 126053, https://doi.org/10.1016/j.conbuildmat.2021.126053.
[21] P. Meriggi, C. Caggegi, A. Gabor, G. de Felice, Shear-compression tests on stone masonry walls strengthened with basalt textile reinforced mortar (TRM), Constr. Build. Mater. 316 (2022, January) 125804, https://doi.org/10.1016/j.conbuildmat.2021.125804.
[22] F. Ferretti, C. Mazzotti, FRCM/SRG strengthened masonry in diagonal compression: experimental results and analytical approach proposal, Constr. Build. Mater. 283 (2021, May) 122766, https://doi.org/10.1016/j.conbuildmat.2021.122766.
[23] A. Incerti, F. Ferretti, C. Mazzotti, FRCM strengthening systems efficiency on the shear behavior of pre-damaged masonry panels: an experimental study, J. Build. Pathol. Rehabilit. 4 (1) (2019, May 23), https://doi.org/10.1007/s41024-019-0053-9.
[24] A. Incerti, A. Bellini, A.R. Tilocca, M. Savoia, Retrofitting with FRCM composites: shear and flexural behaviour of strengthened masonry walls, Key Eng. Mater. 919 (2022, May 11) 80–89, https://doi.org/10.4028/p-6q01h0.
[25] A. Bellini, A. Incerti, C. Mazzotti, Cyclic out-of-plane behavior of FRCM-strengthened masonry walls, Key Eng. Mater. 916 (2022, April 7) 344–351, https://doi.org/10.4028/p-560xb3.
[26] S. Türkmen, B.D. Vries, S. Wijte, J. Ingham, Out-of-plane behaviour of clay brick masonry walls retrofitted with flexible deep mounted CFRP strips and additional single-sided FRCM overlay, Structures 33 (2021, October) 2459–2474, https://doi.org/10.1016/j.istruc.2021.05.061.

[27] J. Donnini, G. Maracchini, S. Lenci, V. Corinaldesi, E. Quagliarini, TRM reinforced tuff and fired clay brick masonry: experimental and analytical investigation on their in-plane and out-of-plane behavior, Constr. Build. Mater. 272 (2021, February) 121643, https://doi.org/10.1016/j.conbuildmat.2020.121643.
[28] C. D'Ambra, G.P. Lignola, A. Prota, E. Sacco, F. Fabbrocino, Experimental performance of FRCM retrofit on out-of-plane behaviour of clay brick walls, Compos. B Eng. 148 (2018, September) 198–206, https://doi.org/10.1016/j.compositesb.2018.04.062.
[29] A. Bellini, A. Incerti, M. Bovo, C. Mazzotti, Effectiveness of FRCM reinforcement applied to masonry walls subject to axial force and out-of-plane loads evaluated by experimental and numerical studies, Int. J. Architect. Herit. 12 (3) (2017, July 14) 376–394, https://doi.org/10.1080/15583058.2017.1323246.
[30] L. Ombres, F. Campolongo, M. Guglielmi, S. Verre, Experimental analysis of the mechanical response of masonry columns partially confined with PBO FRCM (fabric reinforced cementitious mortar) composites, Materials 16 (13) (2023, July 4) 4812, https://doi.org/10.3390/ma16134812.
[31] M. Canestri, F. Ferretti, C. Mazzotti, Confinement of masonry columns through SRG: experimental results and analytical prediction, Procedia Struct. Integr. 44 (2023) 2198–2205, https://doi.org/10.1016/j.prostr.2023.01.281.
[32] V. Alecci, M. De Stefano, S. Galassi, R. Luciano, D. Pugliese, G. Stipo, Influence of different mortar matrices on the effectiveness of FRCM composites for confining masonry columns, J. Test. Eval. 51 (2) (2022, November 22) 20220323, https://doi.org/10.1520/jte20220323.
[33] V. Alecci, M. De Stefano, S. Galassi, R. Magos, G. Stipo, Experimental investigation on the effectiveness of masonry columns confinement using lime-based composite material, Lect. Notes Networks Syst. (2022) 2233–2247, https://doi.org/10.1007/978-3-031-06825-6_215.
[34] V. lecci, M. De Stefano, S. Galassi, R. Magos, G. Stipo, Confinement of masonry columns with natural lime-based mortar composite: an experimental investigation, Sustainability 13 (24) (2021, December 13) 13742, https://doi.org/10.3390/su132413742.
[35] M. Aiello, F. Bencardino, A. Cascardi, T. D'Antino, M. Fagone, I. Frana, L. La Mendola, G. Lignola, C. Mazzotti, F. Micelli, G. Minafò, A. Napoli, L. Ombres, M. Oddo, C. Poggi, A. Prota, G. Ramaglia, G. Ranocchiai, R. Realfonzo, S. Verre, Masonry columns confined with fabric reinforced cementitious matrix (FRCM) systems: a round robin test, Constr. Build. Mater. 298 (2021, September) 123816, https://doi.org/10.1016/j.conbuildmat.2021.123816.
[36] S. Yin, L. Jing, M. Yin, B. Wang, Mechanical properties of textile reinforced concrete under chloride wet-dry and freeze-thaw cycle environments, Cement Concr. Compos. 96 (2019, February) 118–127, https://doi.org/10.1016/j.cemconcomp.2018.11.020.
[37] A. Nobili, Durability assessment of impregnated Glass Fabric Reinforced Cementitious Matrix (GFRCM) composites in the alkaline and saline environments, Constr. Build. Mater. 105 (2016, February) 465–471, https://doi.org/10.1016/j.conbuildmat.2015.12.173.
[38] J. Donnini, Durability of glass FRCM systems: effects of different environments on mechanical properties, Compos. B Eng. 174 (2019, October) 107047, https://doi.org/10.1016/j.compositesb.2019.107047.
[39] F. Ceroni, A. Bonati, V. Galimberti, A. Occhiuzzi, Effects of environmental conditioning on the bond behavior of FRP and FRCM systems applied to concrete elements, J. Eng. Mech. 144 (1) (2018, January), https://doi.org/10.1061/(asce)em.1943-7889.0001375.
[40] I.G. Colombo, M. Colombo, M. di Prisco, Tensile behavior of textile reinforced concrete subjected to freezing–thawing cycles in un-cracked and cracked regimes, Cement Concr. Res. 73 (2015, July) 169–183, https://doi.org/10.1016/j.cemconres.2015.03.001.
[41] N.H. Dinh, S.H. Park, K.K. Choi, Effect of dispersed micro-fibers on tensile behavior of uncoated carbon textile-reinforced cementitious mortar after high-temperature exposure, Cement Concr. Compos. 118 (2021, April) 103949, https://doi.org/10.1016/j.cemconcomp.2021.103949.
[42] H. Asghari, Z. Omeman, M. Noel, H. Hajiloo, Tensile properties of carbon fabric-reinforced cementitious matrix (FRCM) at high temperatures, Structures 55 (2023, September) 85–96, https://doi.org/10.1016/j.istruc.2023.06.025.
[43] M. Messori, A. Nobili, C. Signorini, A. Sola, Effect of high temperature exposure on epoxy-coated glass textile reinforced mortar (GTRM) composites, Constr. Build. Mater. 212 (2019, July) 765–774, https://doi.org/10.1016/j.conbuildmat.2019.04.026.
[44] I. Colombo, M. Colombo, A. Magri, G. Zani, M. di Prisco, Textile reinforced mortar at high temperatures, Appl. Mech. Mater. 82 (2011, July) 202–207, https://doi.org/10.4028/www.scientific.net/amm.82.202.
[45] S.R. Maroudas, C.C.G. Papanicolaou, Effect of high temperatures on the TRM-to-masonry bond, Key Eng. Mater. 747 (2017, July) 533–541, https://doi.org/10.4028/www.scientific.net/kem.747.533.
[46] P.D. Askouni, C.C.G. Papanicolaou, M.I. Kaffetzakis, The effect of elevated temperatures on the TRM-to-masonry bond: comparison of normal weight and lightweight matrices, Appl. Sci. 9 (10) (2019, May 27) 2156, https://doi.org/10.3390/app9102156.
[47] L. Ombres, A. Iorfida, S. Mazzuca, S. Verre, Bond analysis of thermally conditioned FRCM-masonry joints, Measurement 125 (2018, September) 509–515, https://doi.org/10.1016/j.measurement.2018.05.021.
[48] A. Iorfida, S. Candamano, F. Crea, L. Ombres, S. Verre, P. de Fazio, Bond behaviour of FRCM composites: effects of high temperature, Key Eng. Mater. 817 (2019, August) 161–166, https://doi.org/10.4028/www.scientific.net/kem.817.161.
[49] L. Estevan, F. Baeza, F. Varona, J. Pereiro, Effect of high temperature on textile reinforced Mortar-to-masonry bond, Constr. Build. Mater. 393 (2023, August) 132123, https://doi.org/10.1016/j.conbuildmat.2023.132123.
[50] F. Ferretti, A.R. Tilocca, A. Incerti, C. Mazzotti, M. Savoia, Effects of thermal variations on the tensile behavior of FRCM strengthening systems, J. Compos. Construct. 26 (5) (2022, October), https://doi.org/10.1061/(asce)cc.1943-5614.0001241.
[51] H.V. Tran, G.T. Truong, K.K. Choi, Effect of harsh conditions on the tensile behaviour of lap-spliced carbon fiber textile-reinforced mortar (TRM) with different surface treatment methods, Appl. Sci. 9 (15) (2019, July 31) 3087, https://doi.org/10.3390/app9153087.
[52] F. Ferretti, M. Canestri, C. Mazzotti, Effect of Temperature Variations on the Bond Behavior of FRCM Applied to Masonry - Materials and Structures, SpringerLink, 2022, July 13, https://doi.org/10.1617/s11527-022-02002-x.
[53] H. Asghari, M. Noel, H. Hajiloo, Mechanical properties of FRCM at high temperatures, in: Lecture Notes in Civil Engineering, 2022, pp. 499–511, https://doi.org/10.1007/978-981-19-1004-3_41.
[54] P. Kapsalis, T. Tysmans, D. Van Hemelrijck, T. Triantafillou, State-of-the-Art Review on experimental investigations of Textile-Reinforced concrete exposed to high temperatures, J. Compos. Sci. 5 (11) (2021) 290, https://doi.org/10.3390/jcs5110290.
[55] M. Alma'aitah, B. Ghiassi, A. Dalalbashi, Durability of textile reinforced concrete: existing knowledge and current gaps, Appl. Sci. 11 (6) (2021) 2771, https://doi.org/10.3390/app11062771.
[56] Consiglio Superiore dei Lavori Pubblici, Linea Guida per la identificazione, la qualificazione ed il controllo di accettazione di compositi fibrorinforzati a matrice inorganica (FRCM) da utilizzarsi per il consolidamento strutturale di costruzioni esistenti, 2018 (in italian).
[57] EN 998-2, Specification for Mortar for Masonry - Part 2: Masonry Mortar, 2016, 2016.
[58] EN 1015-11:2020, Methods of Test for Mortar for Masonry - Part 11: Determination of Flexural and Compressive Strength of Hardened Mortar, 2020.
[59] EN 772-1, Methods of Test for Masonry Units - Part 1: Determination of Compressive Strength, 2011.
[60] EN 12390-6:2009, Testing Hardened Concrete - Part 6: Tensile Splitting Strength of Test Specimen, 2010.
[61] EN 12390-13, Testing Hardened Concrete - Determination of Secant Modulus of Elasticity in Compression, 2013.
[62] G. de Felice, M.A. Aiello, C. Caggegi, F. Ceroni, S. De Santis, E. Garbin, N. Gattesco, U. Hojdys, P. Krajewski, A. Kwiecień, M. Leone, G.P. Lignola, C. Mazzotti, D. Oliveira, C. Papanicolaou, C. Poggi, T. Triantafillou, M.R. Valluzzi, A. Viskovic, Recommendation of RILEM technical committee 250-CSM: test method for textile reinforced mortar to substrate bond characterization, Mater. Struct. 51 (4) (2018, July 9), https://doi.org/10.1617/s11527-018-1216-x.
[63] ISO 9513-1, Metallic Materials - Calibration of Extensometer Systems Used in Uniaxial Testing, 2012.
[64] S. De Santis, F.G. Carozzi, G. de Felice, C. Poggi, Test methods for textile reinforced mortar systems, Compos. B Eng. 127 (2017, October) 121–132, https://doi.org/10.1016/j.compositesb.2017.03.016.
[65] L. Ascione, G. de Felice, S. De Santis, A qualification method for externally bonded Fibre Reinforced Cementitious Matrix (FRCM) strengthening systems, Composites, Part B 78 (2015) 497–506, https://doi.org/10.1016/j.compositesb.2015.03.079.
[66] M.R. Valluzzi, D.V. Oliveira, A. Caratelli, G. Castori, M. Corradi, G. de Felice, E. Garbin, D. Garcia, L. Garmendia, E. Grande, U. Ianniruberto, A. Kwiecień, M. Leone, G.P. Lignola, P.B. Lourenço, M. Malena, F. Micelli, M. Panizza, C.G. Papanicolaou, A. Prota, E. Sacco, T.C. Triantafillou, A. Viskovic, B. Zając, G. Zuccarino, Round Robin Test for composite- to-brick shear bond characterization, Mater. Struct. 45 (2012) 1761–1791, https://doi.org/10.1617/s11527-012-9883-5.
[67] ISO 10406-1:2014, Fibre-reinforced Polymer (FRP) Reinforcement of Concrete - Test Methods - Part 1: FRP Bars and Grids, 2014.